

Electronic and Structural Aspects of Spin Transitions Observed by Optical Microscopy. The Case of $[\text{Fe}(\text{ptz})_6](\text{BF}_4)_2$

Christian Chong,[†] Haritosh Mishra,[†] Kamel Boukheddaden,[†] Stéphane Denise,[†] Guillaume Bouchez,[†] Eric Collet,[‡] Jean-Claude Ameline,[‡] Anil D. Naik,[§] Yann Garcia,[§] and François Varret^{*,†}

Groupe d'Etude de la Matière Condensée, CNRS-Université de Versailles UMR 8635, 45 avenue des Etats-Unis, 78035 Versailles cedex, France, Institut de Physique de Rennes, CNRS-Université de Rennes 1, campus de Beaulieu, 35042 Rennes cedex, France, and Unité de Chimie des Matériaux Inorganiques et Organiques, Département de Chimie, Université Catholique de Louvain, Place L. Pasteur 1, 1348 Louvain-la-Neuve, Belgium

Received: November 19, 2009; Revised Manuscript Received: December 18, 2009

The colorimetric analysis of images recorded with an optical microscope during the onset of the spin crossover transformation allows monitoring separately the involved electronic and structural aspects, through the separation of resonant absorption and scattering effects. Complementary information can also be obtained by using the polarized modes of the microscope. These potentialities are illustrated by the observation of $[\text{Fe}(\text{ptz})_6](\text{BF}_4)_2$ single crystals during the onset of the thermal transitions in the 110–140 K range. We characterized the interplay between the electronic ($\text{HS} \leftrightarrow \text{LS}$) and structural (order \leftrightarrow disorder) transformations. Elastic stresses and mechanical effects (hopping, self-cleavage) generated by the volume change upon electronic transition are also illustrated, with their impact on the photoswitching properties of the crystals.

Introduction

In a previous paper,¹ we introduced the colorimetric method for investigating the spin-crossover transformations by means of optical microscopy, on the well-known spin transition compound $[\text{Fe}(\text{ptz})_6](\text{BF}_4)_2$ (ptz = 1-propyl-tetrazole) here abbreviated as Fe-ptz. We mainly considered quasi-static transformations such as the low-temperature photoexcitation of the system, that is, the low-spin (LS) \rightarrow high-spin (HS) phototransformation termed light-induced excited spin state trapping (LIESST),^{2,3} and the subsequent thermal relaxation of the system. Thanks to crucial improvement on the synthesis of high-quality crystals and of the thermal contact between the crystal and temperature sensor, now we can follow carefully the phase transitions of the system, with minimized temperature gradients and without exerting any mechanical stress on the crystal, a major requirement due to sensitivity of the spin transitions to pressure effects (see refs 4 and 5 for appropriate bibliography). The present report is devoted to the observation of the thermal transition in the quoted compound and to the description of side effects generated by the volume change associated with the electronic transformation. Fe-ptz undergoes a structural transition in the vicinity of the spin transition, and the interplay between the two kinds of transitions was previously followed by X-ray diffraction^{6,7} and optical spectroscopy.⁸ The present data corroborate these previous works and reveal some spatial aspects of the transition mechanism.

Results and Discussion

Optical Microscope Approach. We used in transmission mode a standard optical microscope Laborlux 12 pol from Leica



Figure 1. The helium-tight cell designed for optical microscopy.

equipped with CCD camera Sony Digital Hyper HAD SSC-DC38P. We automatically recorded the PC screen by using the CamStudio software. The 8×6 mm detector contained 756×564 pixels. For obtaining complete images of the crystal, we used an objective $\times 7$, NA = 0.12, leading to a resolution limit of $\sim 2.5 \mu\text{m}$ which compares to the CCD interpixel distance $\sim 3.3 \mu\text{m}$ (reported to the object field). We show in Figure 1 the helium-tight cell, which was loaded in a glovebox.

Fe-ptz crystals were grown at the Louvain University, using a method described in ref 1. They were large, in the shape of triangles, and we had to cut them into pieces for fitting in the field of the microscope. In Figure 2, we show typical images of the LS and HS states, recorded in transmission geometry using backward illumination by tungsten halogen lamp, provided by the microscope. At low temperature (in the range 7–10 K), illumination by the microscope induced a complete phototransformation of the crystal

* Corresponding author. Fax: (33) 1 39 25 46 52. E-mail: varret_francois@yahoo.fr

[†] UMR-8635.

[‡] UMR-6251.

[§] Université Catholique de Louvain.

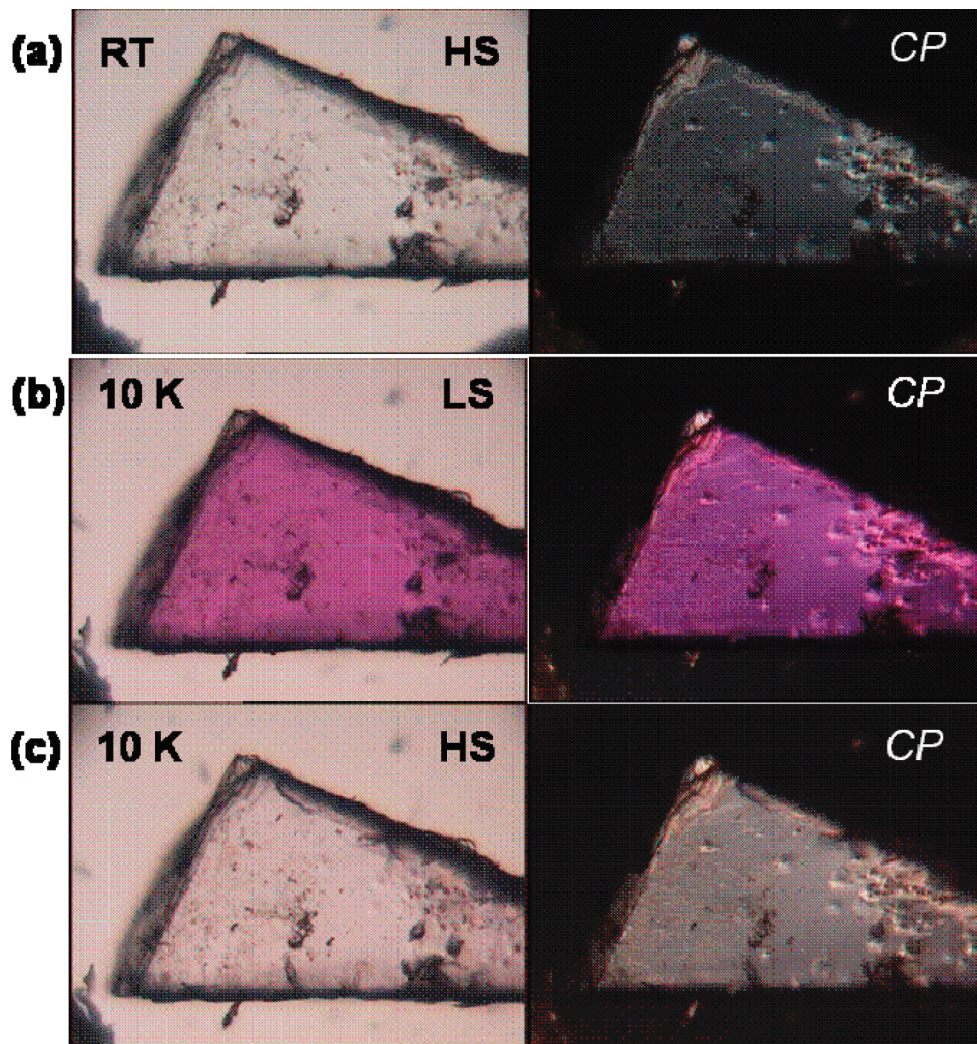


Figure 2. Fe-ptz in the $\bar{R}\bar{3}$ structural state: (a) at room temperature, (b) in the (rapidly cooled) LS state, and (c) in the HS photoexcited state. The full horizontal scale is ~ 2.64 mm. CP = cross polarizer geometry.

within typically 1 h. The phototransformation of fresh crystals was always homogeneous at the resolution of the microscope, in agreement with previous neutron diffraction investigations,⁹ which obviously had a higher resolution. In addition, the uniformly black images obtained between crossed polarizers showed the high structural quality of the fresh crystals.

The colorimetric method¹ is illustrated in Figure 3. It is based on the measurements of optical densities (ODs) associated with the three kinds of pixels (green, red, blue). An optical density is defined as the decimal logarithm of the ratio of incident/transmitted intensities, $OD = \log_{10}(I_0/I)$. In transmission geometry, I_0 merely is the bright field intensity, and I can be determined, either locally, or in average over a defined area of the crystal.

It is clear from a simple glance at Figure 3 that the green OD is tightly correlated to the LS fraction in the crystal (actually, proportional to), while the other two ODs are much less sensitive to the variation of spin fraction and their variations are practically negligible. However, we observed in ref 1 that the red and blue ODs exhibited sizable variations associated with aging effects in the crystal, that is, with the onset of cracks or defects. Such an increase was assigned to scattering of light, and was independently observed as a *raise of the baseline of the optical spectra* in Hauser's crucial works on the optical investigations of spin transitions.¹⁰ This scattering effect was attributed to the presence of domains at the transition, and reached an unprecedented magnitude

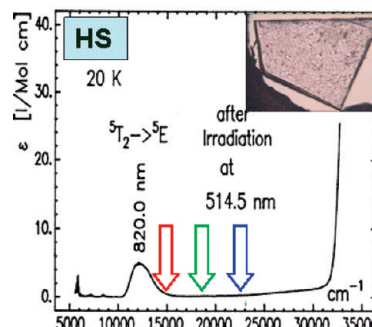
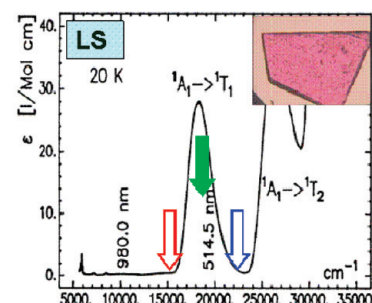


Figure 3. Absorption spectra of Fe-ptz in the HS and LS states (after ref 10), with the location of the spectral sensitivity of the RGB pixels.

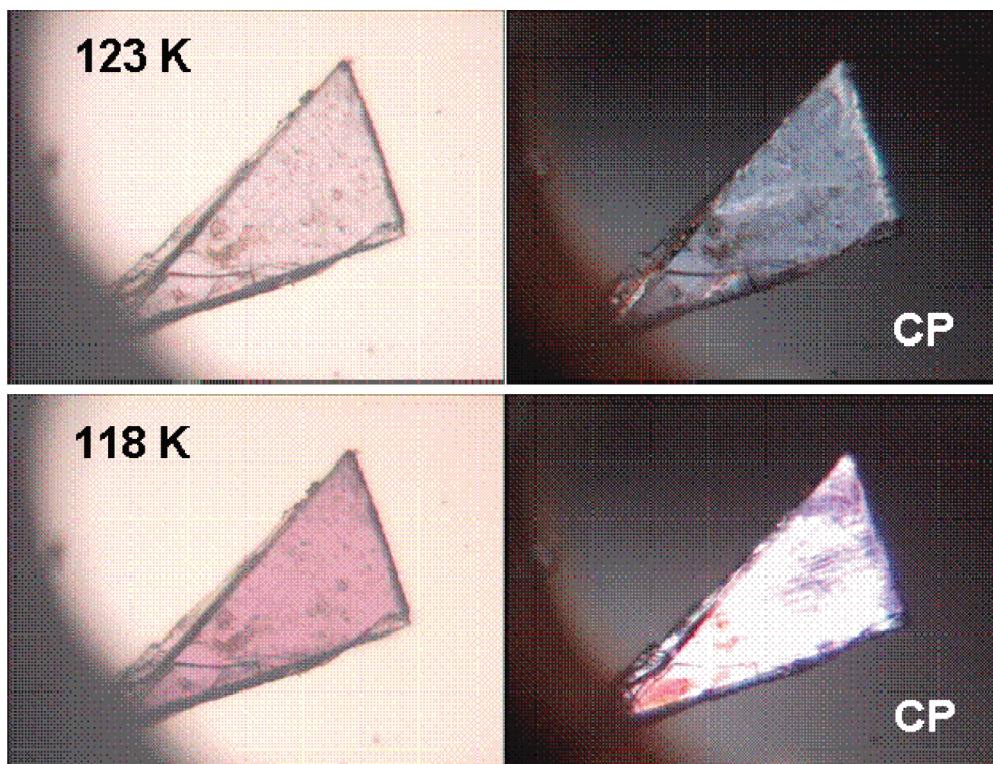


Figure 4. A small piece of the Fe-ptz crystal, during slow cooling through the spin transition (top, HS- $R\bar{3}$; bottom, LS- $R\bar{3}dis$). The crystal size is ~ 2.0 mm at the largest edge.

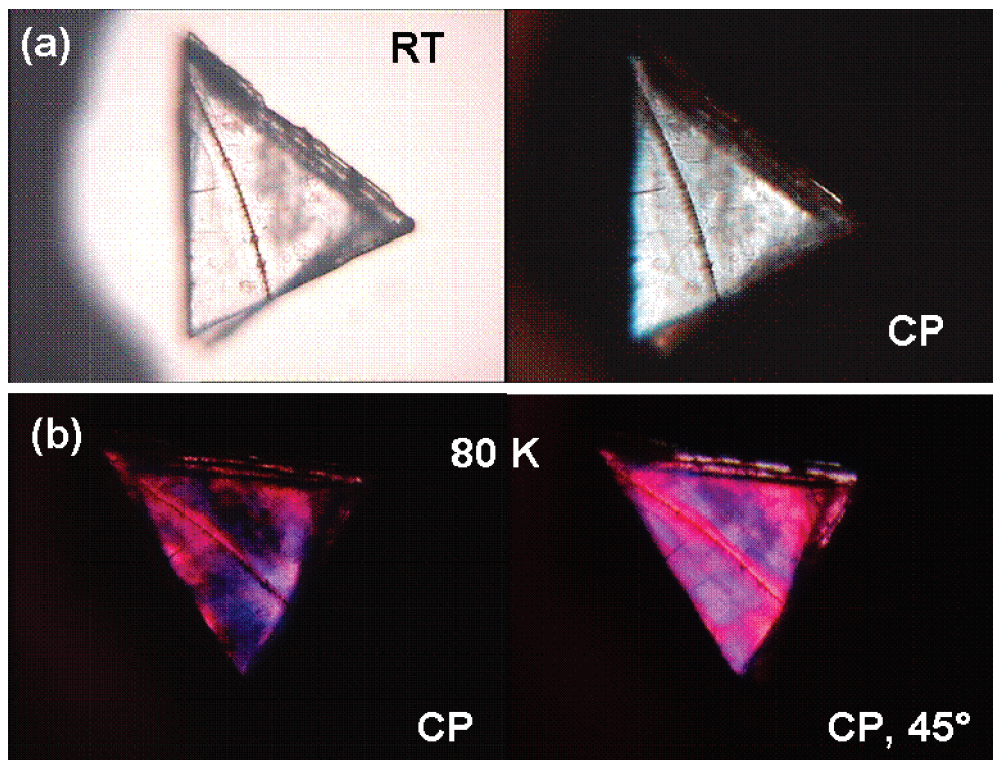


Figure 5. (a) A scratched piece of Fe-ptz crystal, exhibiting sizable scattering of light at room temperature. (b) The same crystal at low temperature, in the LS- $R\bar{3}$ state, after photoexcitation and relaxation, for two selected orientations of the crossed polarizers (rotated by 45°). The crystal size is ~ 1.6 mm at the largest edge.

in the case of $[Fe(bbtr)_3](ClO_4)_2$ ($bbtr = 1,4$ -di(1,2,3-triazol-1-yl)butane),¹¹ a polymeric counterpart of the Fe-ptz system. To summarize, any simultaneous increase of all ODs has to be assigned to scattering of light.

This new approach to the scattering effect can be conveniently completed by an investigation between crossed polarizers.

Indeed, the scattered light is no longer fully polarized, and depolarizing areas can be shown as bright areas between crossed polarizers, with a small (or negligible) angular dependence with respect to the crystal orientation.

In Figure 4, we show a Fe-ptz crystal in the HS state and in a LS state obtained by slow cooling through the spin transition,

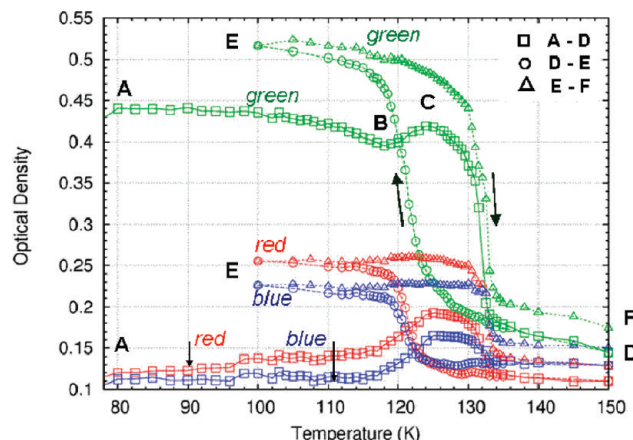


Figure 6. Successive transformations of a Fe(ptz) quenched crystal, during successive heating, cooling, and reheating stages, at the temperature scan rate ± 0.1 K/min (successive labels from A to F). The optical density data are plotted with their respective colors.

which according to refs 6 and 7 induces a structural transformation from the $R\bar{3}$ space group to an $R\bar{3}$ -type disordered phase, abbreviated here as $R\bar{3}\text{dis}$. This figure should be compared to Figure 2. Between crossed polarizers (bottom, right image), the crystal is no longer dark, with a transmitted intensity which essentially does not depend on the orientation of the crystal. It is assigned to scattering of light due to micrometer-size domains created by the structural transformation. As a matter of fact, the cross-polarization images also provide information on an eventual birefringence of the crystal, through colored areas, as shown in Figure 5. Birefringence is established by the angular dependence of the colored patterns, when the crystal is rotated with respect to the polarization direction. The occurrence of birefringence may be due to disorientation of the crystal, symmetry lowering of the optical properties resulting from structural phase change, or elastic stresses. In the present case, birefringence effects are assigned to the presence of elastic stresses, presumably associated with the scratch which occurred

when cutting the crystal, that is clearly seen in Figure 5. In a further section, we shall report that such stresses can also be obtained by an unwilling structural transformation, sometimes observed in aged crystals. These alternative explanations can be distinguished by determining the relaxation properties of the photoexcited HS state, which are drastically affected by the structural transformation. The light scattering effect will be used in the following for characterizing the presence of the $R\bar{3}\text{dis}$ state.

Investigation of Fe-ptz Crystals. The Fe-ptz crystals were rapidly cooled (at ~ 20 K/min) in order to retain the ordered $R\bar{3}$ structure in the low-temperature initial state. It is known from X-ray investigation^{6,7} and other techniques¹² that (i) upon heating at 120 K, the LS phase undergoes a structural change toward the $R\bar{3}\text{dis}$ phase, before the spin transition takes place, and (ii) subsequent temperature cycling around the transition reversibly induces the coupled transformations $\text{LS}-R\bar{3}\text{dis} \leftrightarrow \text{HS}-R\bar{3}$. We followed here the same thermal history, at a constant rate of 0.1 K/min, and determined the OD values, which are reported in Figure 6.

Figure 6 is highly informative. Let us first concentrate on the first heating branch. The initial $\text{LS}-R\bar{3}$ state is characterized by a large green OD (typical for the LS state) and negligible scattering of light. Upon temperature increase, the electronic transformation exhibits first a shy start (slight decrease in green OD) shortly followed by a simultaneous increase in all ODs at ~ 118 K. Scattering of light takes place and peaks around 125 K, due to the onset of the structure transition, $R\bar{3} \rightarrow R\bar{3}\text{dis}$. Upon further heating, all ODs exhibit a rapid decrease slightly above 130 K, due to the joined spin and structure transition $\text{LS}-R\bar{3}\text{dis} \rightarrow \text{HS}-R\bar{3}$. We concluded that the scattering of light is merely associated with the presence of the disordered phase. Further thermal variations of the system evidenced the hysteretic $\text{HS}-R\bar{3} \leftrightarrow \text{LS}-R\bar{3}\text{dis}$ joined transformation. Inspection of the complete figure shows that the structural transformation $R\bar{3} \rightarrow R\bar{3}\text{dis}$ on the first heating stage was not complete. This can be assigned to the kinetic character of the structural transformation, reported in refs 6 and 7.

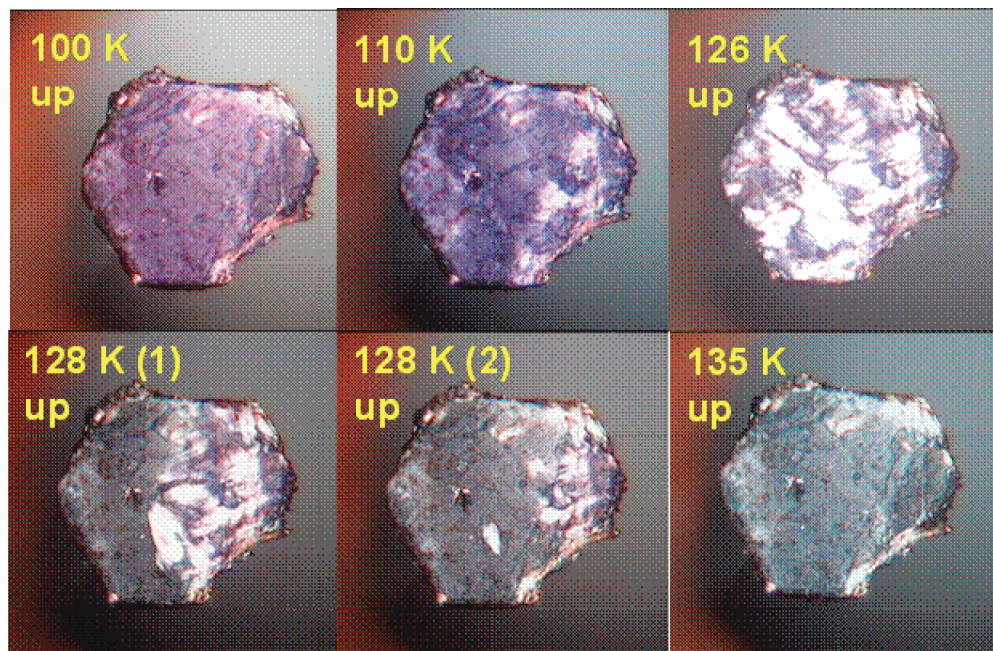


Figure 7. Fe-ptz, another crystal, thermally quenched, CP images selected during the first heating, leading to the successive transformations $\text{LS}-R\bar{3} \rightarrow \text{LS}-R\bar{3}\text{dis} \rightarrow \text{HS}-R\bar{3}$ in the top and bottom parts, respectively. The successive images at 128 K labeled (1) and (2) are separated by ~ 20 s. The crystal size is ~ 1.4 mm for the largest diameter.

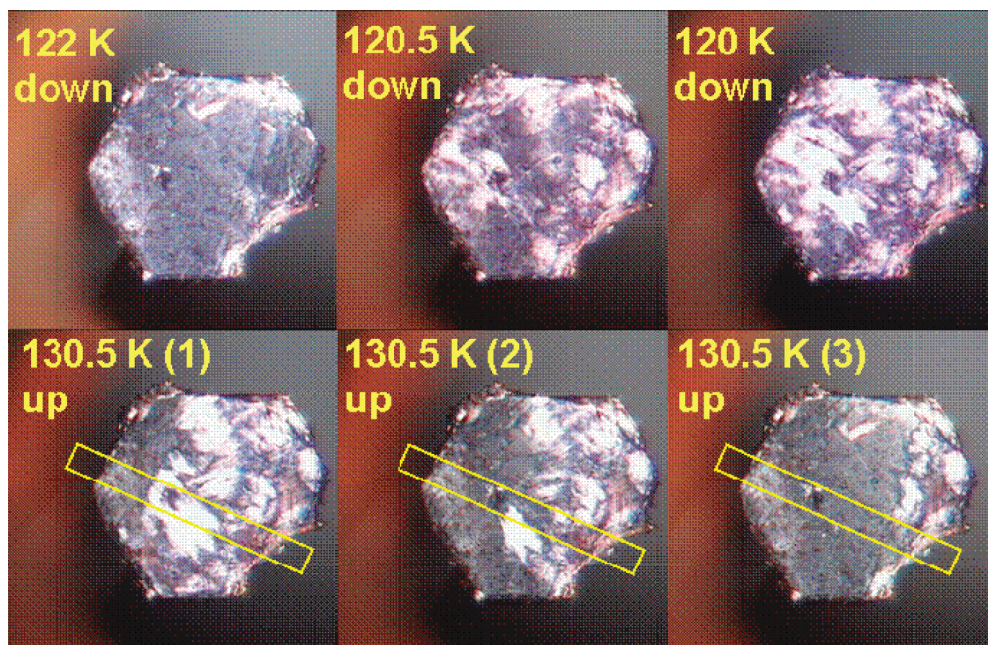


Figure 8. Fe-ptz, subsequent CP images recorded during further cooling (top) and heating (bottom), during the hysteretic $\text{HS}-\bar{R}^3 \leftrightarrow \text{LS}-\bar{R}^3\text{dis}$ joined transformation. The rectangular frame deals with the kinetic analysis performed in a further section (Figure 11).

Details on the spatiotemporal aspects of the phase transformations can be obtained by a careful inspection of the images, including those recorded between crossed polarizers (CP). As a matter of fact, we observed that the character of the nucleation and growth processes was not identical in all crystals, and obviously depending on the quality of the crystals. The detailed investigation reported here in Figures 7 and 8 was performed on a crystal which already exhibited some scattering effects at room temperature. We show in Figure 7 the crossed-polarization images associated with the first heating stage. The crystal initially was in the quenched $\text{LS}-\bar{R}^3$ state (100 K). Upon heating up to 126 K (top Figure 7), it exhibited growing white areas which correspond to nucleation of the $\text{LS}-\bar{R}^3\text{dis}$ phase, at least 10 K below the temperature (120 K) where the complete transformation is reported to occur within approximately half an hour.^{6,7} Although the temperature scan rate 0.1 K/min should have let the crystal a sufficient time around 120 K for a complete structural transformation, we actually observed that the latter remained incomplete. At the present time, we may only speculate that structural factors such as the size and quality of the crystals may impact the kinetics of the structural transformation.

Upon further heating (bottom, Figure 7), the white areas progressively vanished, with a diffuse forehead, which rapidly crossed over the crystal from left to right. With the help of some bright field images (not shown), we easily observed that the $\text{HS}-\bar{R}^3$ phase progressively substituted the $\text{LS}-\bar{R}^3\text{dis}$ phase: the black area typical for the \bar{R}^3 state rapidly covered the image from left to right. To summarize, the second transformation on heating— involving spin and structure—is the faster one. The linear character of the diffuse forehead of this transformation reveals the presence of a small temperature gradient in the crystal, while the local features are assigned to slight variations of the structural qualities through the crystal involving short-range elastic stresses.

We show in Figure 8 further CP images recorded during the subsequent cooling and heating of the crystal through the hysteretic $\text{HS}-\bar{R}^3 \leftrightarrow \text{LS}-\bar{R}^3\text{dis}$ joined transformation. Upon cooling (top, Figure 8), the transition proceeds by a rather slow

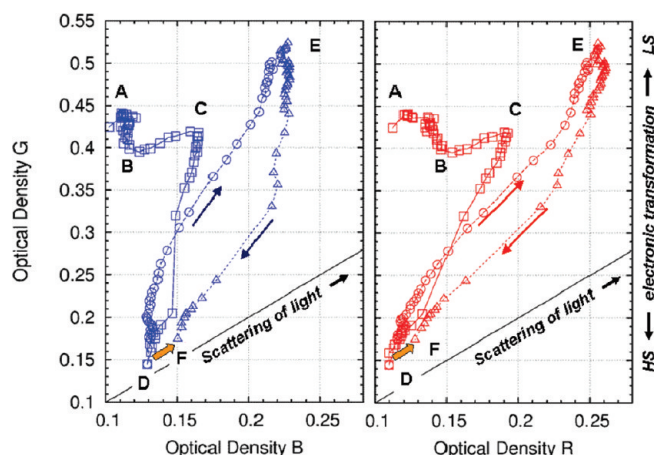


Figure 9. Fe-ptz, the correlation plots of the optical density data at the thermal transition. Labels A–F are used for correspondence to Figure 6.

nucleation and growth process, scattered over various parts of the crystal. During the heating stage, we observed the crystal at 130.5 K as a function of time. We followed the diffuse forehead of the \bar{R}^3 HS state, moving from left to right on the images. It is worth noting that the presence of a tiny temperature gradient was needed for such an observation. The diffuse character of this forehead drastically differs from the sharp one we recently observed at the thermal transition of the polymeric spin crossover compound $[\text{Fe}(\text{btr})_2(\text{NCS})_2] \cdot \text{H}_2\text{O}$. Indeed, by optical microscopy,^{13,14} we observed the nucleation of a single LS domain and the rapid propagation of a clear-cut domain wall in agreement with the expectations based on diffraction data.¹⁵

The interplay between structural and electronic transformations at the thermal transition can be further analyzed. In a first step, the data of Figure 6 can be reported in terms of correlation plots of various ODs; see Figure 9. These plots can be considered as flow diagrams for transformations involving two order parameters. In a first approach, the electronic transformation leads to vertical displacements on the figures, while the

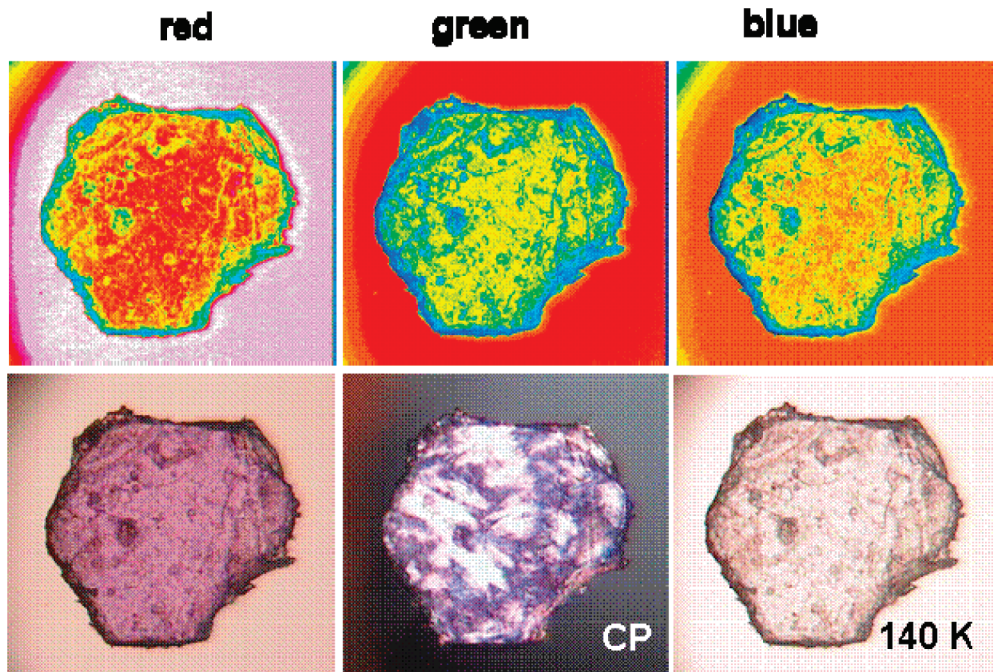


Figure 10. Fe-ptz in the $LS-R\bar{3}dis$ state (116 K). Top row = R, G, B maps. Bottom row: the bright field and CP images at 116 K and the bright field image in the $HS-R\bar{3}$ state (140 K).

scattering effect associated with the structural transformation leads to displacements parallel to the first bisector (due to equal variations of all densities). According to this viewpoint, the plots of Figure 9 can be described as follows: upon the first heating, the $LS-R\bar{3}$ phase undergoes a partial and progressive electronic transformation [A–B] before an almost pure but also incomplete structural transformation [B–C]. This is followed by a combined process [C–D] leading to the $HS-R\bar{3}$ phase. Upon subsequent cooling [D–E] and heating [E–F], it can be observed that the structure transformation is delayed with respect to the electronic transformation; actually, it starts later but ends sooner, an effect which illustrates the different kinetics of these joined transformations. The irreversible effects observed after complete cycling of the thermal transition (shown by block arrows) are consistent with a purely structural effect. The differences between the red and blue data might provide through adequate models some information on the size of the structural domains responsible for the scattering of light.

A local insight into the correlation between structural and electronic transformations can be expected from image processing. In Figure 10, we show the OD maps of the R, G, and B pixels for the $LS-R\bar{3}dis$ state (116 K, label E in Figures 6 and 9). These maps are extremely similar in shape. They are hardly correlated to the image recorded between crossed polarizers but rather to the image in the $HS-R\bar{3}$ state. They mainly result from the presence of defects and edges which are the basic ingredients of any contrasted image. We therefore concluded that the structural quality of the present crystal was not sufficient for providing reliable maps of the spin state, which are required for observing the awaited like-spin domain patterns.

The CP images are much more informative. Although their quantitative analysis is certainly much more complex, they provide clear information on the spatiotemporal development of the structural transformation. We actually followed in detail the isothermal transformation at 130.5 K, some images of which were shown in the bottom row of Figure 8. We measured the section of the total intensity map along a rectangular area conveniently oriented, and the resulting profiles are shown in

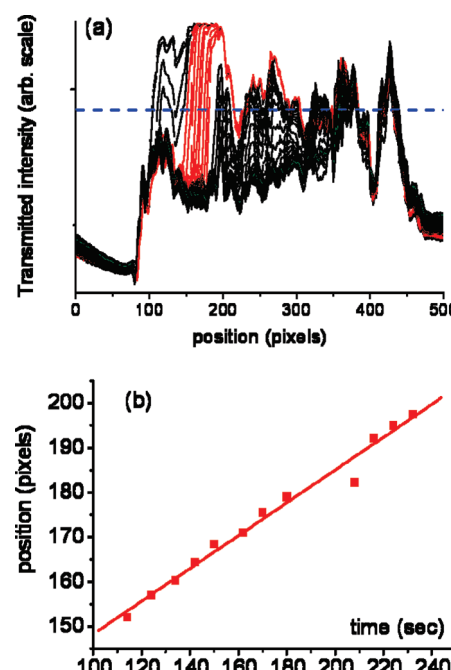


Figure 11. Fe-ptz during isothermal observation at 130.5 K: (a) Successive profiles of the transmitted total intensity ($R+G+B$), along the rectangle shown in the bottom part of Figure 8, with 1 pixel $\sim 3.1 \mu\text{m}$. (b) Determination of the velocity of the diffuse forehead, during the rapid propagation stage, from the plot of the intersect of the red curves with the horizontal line shown in part a, as a function of time. Linear regression yields 0.37 (2) pixel/s ~ 1.1 (1) $\mu\text{m}/\text{s}$.

Figure 11. The motion of the diffusion forehead of the $R\bar{3}dis \leftrightarrow R\bar{3}$ transformation is easily followed. The propagation velocity during the whole process is far from constant, but in the rapid stage shown in Figure 11 (red curves), it could be estimated rather accurately, ~ 1.1 (1) $\mu\text{m}/\text{s}$. The nonconstant character of the velocity is assigned to the presence of local stresses which oppose the propagation of the phase transformation. We observed a similar influence of elastic stresses upon

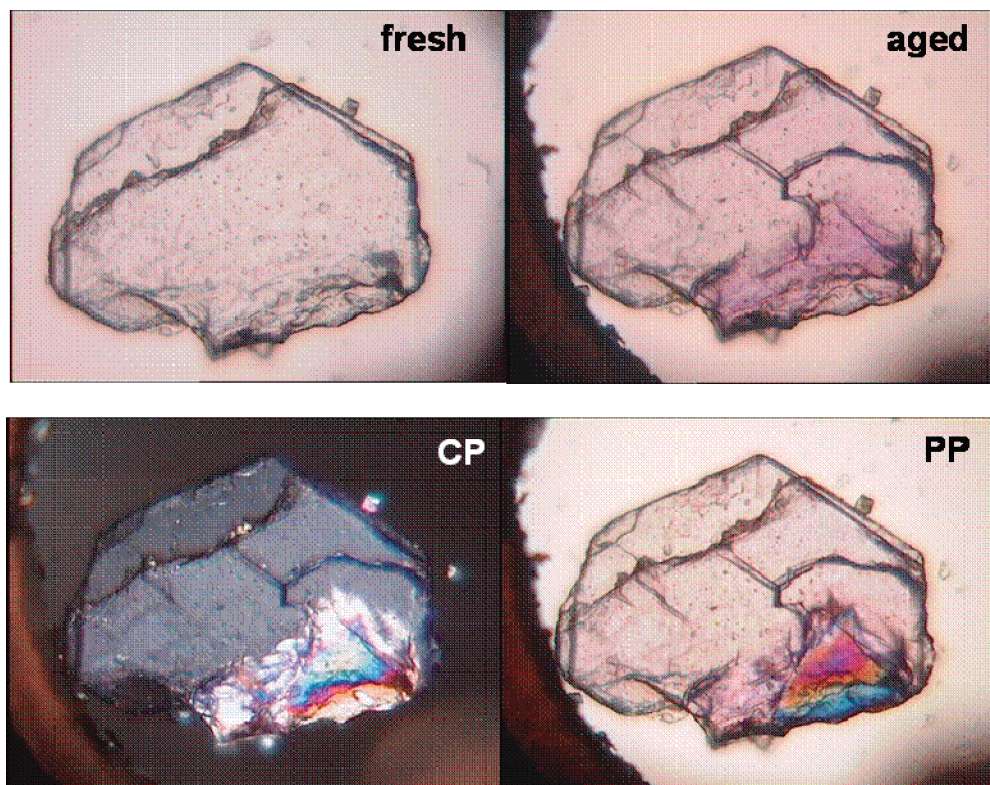


Figure 12. Fe-ptz, the reluctant character of an aged crystal, is correlated to the presence of elastic stresses (colored area) resulting from contamination by the $R\bar{3}dis$ disordered phase (white areas in CP mode). PP = parallel polarizers.

the spin transition of $[Fe(btr)_2(NCS)_2] \cdot H_2O$ ($btr = 4,4'-bis-1,2,4$ -triazole) through recent optical microscope investigations.^{13,14}

The present method enabled us to elucidate the aging mechanism which led to hindering of the photoexcitability of the Fe-ptz crystals; see Figure 12. While the fresh crystal could be totally photoexcited at low temperature, the aged crystal (after performing several thermal and optical switching cycles) exhibited a reluctant area, which remained in the LS state when the remainder of the crystal reached the HS photoexcited state. Observed in polarized mode, the reluctant area displayed orientation dependent colors surrounded by white areas; see bottom figure. The reluctant character of the colored area is therefore assigned to the presence of elastic stresses due to contamination by the $R\bar{3}dis$ phase.

While observing another piece of the large crystal, we could evidence a spectacular self-cleavage effect due to the presence of internal stresses. We illustrate in Figure 13 the behavior of the crystal under slow heating after thermal quenching. Self-cleavage occurred at 113 K, under the effect of elastic stresses (colored areas) due to the early nucleation of the disordered structural phase. Hopping of the crystal was also evidenced during the subsequent $LS - R\bar{3}dis \rightarrow HS - R\bar{3}$ joined transformation, due to the effect of crystal expansion, and the rapid diffusion of the transition foreheads was also observed in agreement with the previous conclusions. The complex character of the spin domain pattern visible at 138 K can be associated with the presence of cracks. Finally, the elastic stresses were released in the $HS - R\bar{3}$ state. It is worth pointing out the obvious role of elastic stresses in the transition mechanism. These elastic effects are certainly a crucial ingredient for realistic models of the thermal transition.^{16,17} As a matter of fact, self-cleavage and hopping of the crystals were also observed at low temperature during the photoexcitation process and seem to be inherent to the effect of any inhomogeneous factor such as temperature gradient or inhomogeneous photoexcitation.

The last example deals with the low-temperature photoexcitation of Fe(ptz). The photoexcitation process was repeated many times for the needs of a complete investigation of the photo-switching and relaxation properties of the system, and experiments performed with a fresh crystal, conveniently quenched, exhibited a monotonous and uniform increase of the HS fraction, with sometimes slight motions or hopping of the crystals. However, using aged crystals, we often observed a chaotic-like behavior during photoexcitation in some parts of the crystal. Observation of such an erratic effect in real time was spectacular, and here we try to illustrate it at best using static figures. In Figure 14, we show the crystal at typical steps of the phototransformation: initial $LS - R\bar{3}$ state, hopping, self-cleavage and onset of stresses, photostationary state (mainly $HS - R\bar{3}$). We show in Figure S1 (Supporting Information) the profile of the green OD measured along a selected area (defined by the narrow rectangular frame in Figure 14) at different times. The other two ODs exhibit similar variations and suggest a structural origin of these erratic variations. This origin is confirmed by a detailed inspection of the data, reported in the Supporting Information. The final Figure 15 illustrates the nonmonotonic behavior of the system, reminiscent of a Barkhausen-like effect previously observed in our previous photomagnetic study.¹⁸ The complete analysis of the spatiotemporal aspects of this erratic (chaotic?) evolution was out of the scope of the present report.

Conclusion

We have shown that the colorimetric investigation in three colors (RGB) enabled separation of the optical absorption effects associated with the spin fractions from the scattering effects associated with the onset of the disordered structural phase. Investigation with crossed polarizer geometry provided complementary information on the scattering effects and on birefringence induced by elastic stresses. The combination of both

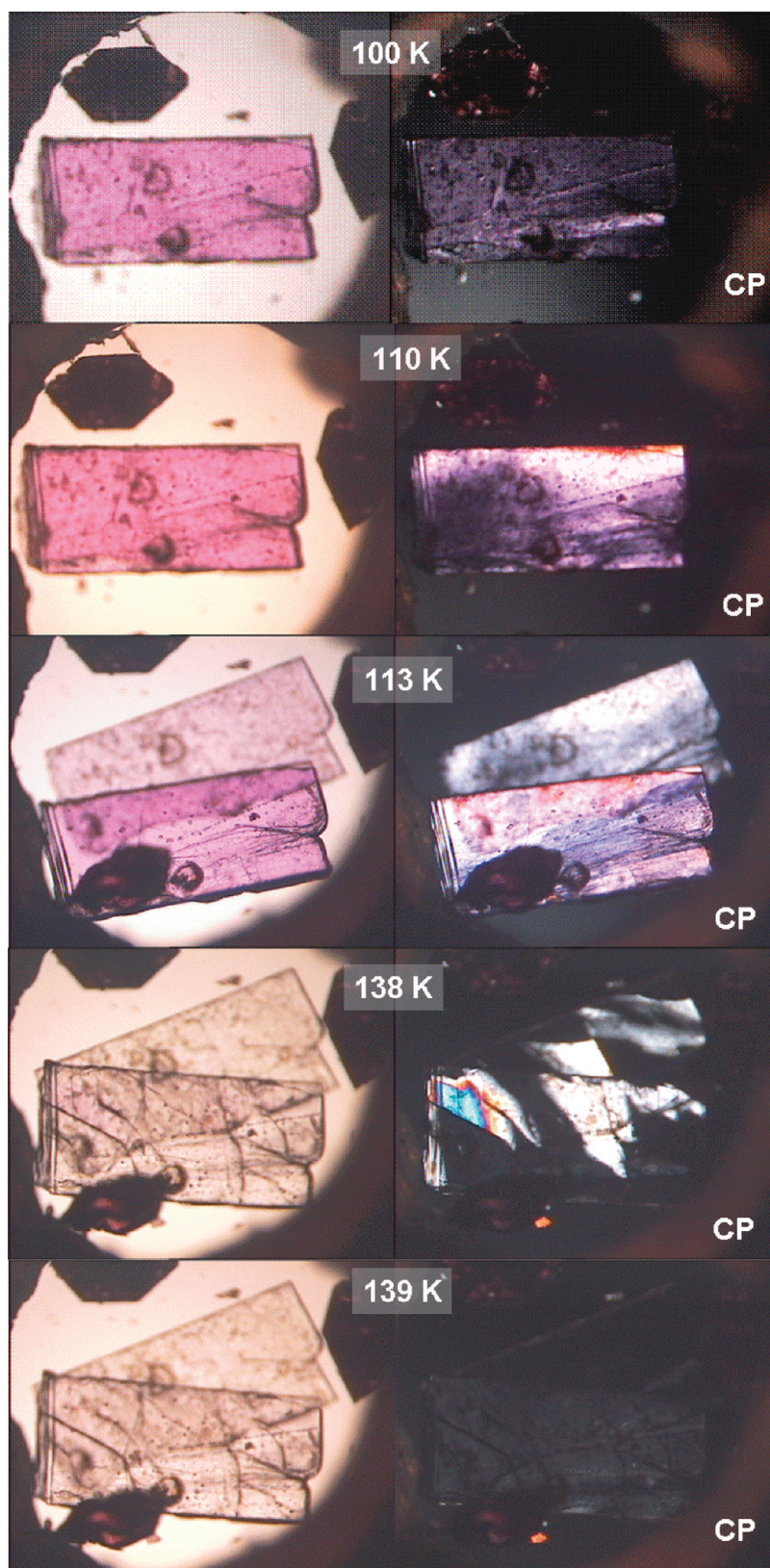


Figure 13. Self-cleavage and hopping effects in another piece of Fe(ptz) crystal, during the first heating after thermal quench. The crystal was 1.6 mm long. The dark polygons are $[\text{Fe}(\text{btr})_2(\text{NCS})_2] \cdot \text{H}_2\text{O}$ for a preliminary investigation which will be reported separately.

techniques enabled us to elucidate several aspects of the physical mechanisms involved in the thermo- and photoswitching properties of the spin-crossover compound $[\text{Fe}(\text{ptz})_6](\text{BF}_4)_2$, viz., the interplay between the electronic and structural transformations at the thermal transition, the origin of elastic stresses, and their impact on the photoswitching properties.

Acknowledgment. We acknowledge financial support from CNRS, Versailles and Rennes Universities, Conseil Régional d'Ile de France (C'Nano, project COLLE), the European Network of Excellence MAGMANet (FP6-515767-2), the IAP-VI (P6/17) INANOMAT and the Fonds National de la Recherche Scientifique (FRFC No 2.4508308). We are grateful to Profs.

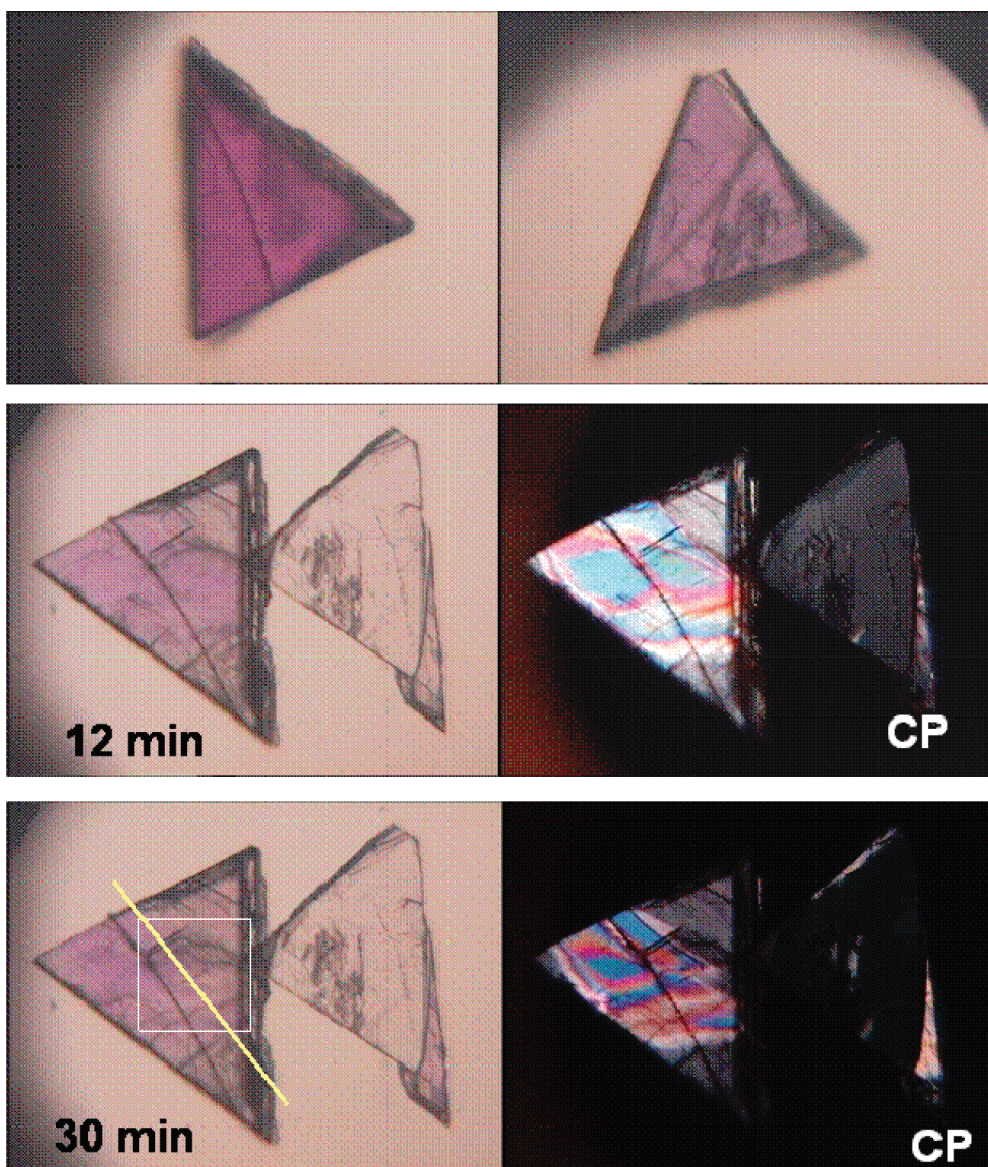


Figure 14. Fe-ptz, the scratched crystal under the first low-temperature (10 K) irradiation. The erratic behavior is mainly observed in the framed square area. The narrow rectangular area was used for determining the OD profiles reported in Figure S1 (Supporting Information), and the spatiotemporal plot reported in Figure 15.

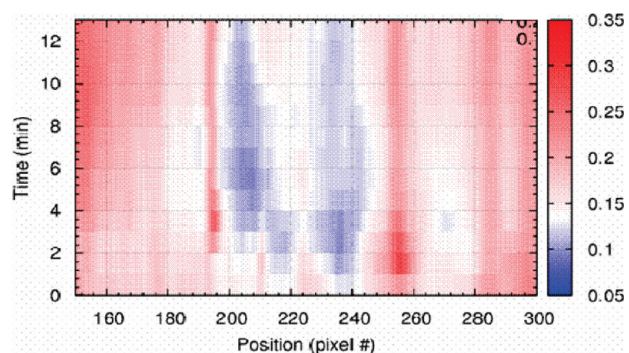


Figure 15. Fe-ptz, the temporal dependence (vertical axis) of the green OD along the central part of the selected rectangle (horizontal axis), illustrating the spatiotemporal variations during the nonmonotonous transformation of the crystal. The dark red areas correspond to the sharp peaks shown in Figure S1 of the Supporting Information.

H. Cailleau (Université de Rennes) and A. Hauser (Université de Genève) for helpful discussions.

Supporting Information Available: Figures showing typical OD profiles determined during the photo-excitation process and flow diagrams at selected positions (determined from Figure 14). This material is available free of charge via the Internet at <http://pubs.acs.org>.

References and Notes

- (1) Goujon, A.; Varret, F.; Boukhechdaden, K.; Chong, C.; Jeftic, J.; Garcia, Y.; Naik, A. D.; Ameline, J. C.; Collet, E. *Inorg. Chim. Acta* **2008**, *361*, 4055.
- (2) Decurtins, S.; Gütlich, P.; Köhler, C. P.; Spiering, H.; Hauser, A. *Chem. Phys. Lett.* **1984**, *139*, 1.
- (3) Decurtins, S.; Gütlich, P.; Haselbach, K. M.; Spiering, H.; Hauser, A. *Inorg. Chem.* **1985**, *24*, 2174.
- (4) Jeftic, J.; Romstedt, H.; Hauser, A. *J. Phys. Chem. Solids* **1996**, *57*, 1743.
- (5) Codjovi, E.; Menendez, N.; Jeftic, J.; Varret, F. *C. R. Acad. Sci. 2001*, *4*, 181.
- (6) Kusz, J.; Gütlich, P.; Spiering, H. *Top. Curr. Chem.* **2004**, *234*, 129.
- (7) Jung, J.; Schmitt, G.; Wiehl, L.; Hauser, A.; Knorr, K.; Spiering, H.; Gütlich, P. *Z. Phys. B* **1996**, *100*, 523.
- (8) Jeftic, J.; Hauser, A. *J. Phys. Chem. B* **1997**, *101*, 10262.
- (9) Goujon, A.; Gillon, B.; Gukasov, A.; Jeftic, J.; Nau, Q.; Codjovi, E.; Varret, F. *Phys. Rev. B* **2003**, *67*, 220401 (R).

- (10) Hauser, A. *J. Chem. Phys.* **1991**, *94*, 2741.
(11) Krivokapic, I.; Enachescu, C.; Bronisz, R.; Hauser, A. *Inorg. Chim. Acta* **2008**, *361*, 3616.
(12) Lemée-Cailleau, M. H.; Ecolivet, C.; Ouladdiaf, B.; Moussa, F.; Jeftic, J.; Létard, J. F. *J. Magn. Magn. Mater.* **2007**, *310*, 1792.
(13) Varret, F. European Conference on Molecular Magnetism (EC-MM09, Wroclaw, Poland, Oct 2009).
(14) Varret, F.; Chong, C.; Mishra, H.; Boukhechda, K.; Haasnoot, J. G. Manuscript in preparation.
(15) Pillet, S.; Legrand, V.; Souhassou, M.; Lecomte, C. *Phys. Rev. B* **2006**, *74*, 140101 (R).
(16) Enachescu, C.; Stoleriu, L.; Stancu, A.; Hauser, A. *Phys. Rev. Lett.* **2008**, *102*, 257204.
(17) Nicolazzi, W.; Pillet, S.; Lecomte, C. *Phys. Rev. B* **2008**, *78*, 174401.
(18) Varret, F.; Boukhechda, K.; Chong, C.; Goujon, A.; Gillon, B.; Jeftic, J.; Hauser, A. *Eur. Phys. Lett.* **2007**, *77*, 30007.

JP910999Y